Tunable Low-Field Magnetoresistance in (La0.7Sr0.3MnO3)0.5:(ZnO)0.5 Self-Assembled Vertically Aligned Nanocomposite Thin Films

ARTICLE *in* ADVANCED FUNCTIONAL MATERIALS · JULY 2011

Impact Factor: 11.81 · DOI: 10.1002/adfm.201002746

9 AUTHORS, INCLUDING:

Aiping Chen
Los Alamos National Laboratory
57 PUBLICATIONS **558** CITATIONS
SEE PROFILE

Xinghang Zhang
Texas A&M University
185 PUBLICATIONS **3,285** CITATIONS
SEE PROFILE

Quanxi Jia
Los Alamos National Laboratory
564 PUBLICATIONS **10,573** CITATIONS
SEE PROFILE

Judith MacManus-Driscoll
University of Cambridge
392 PUBLICATIONS **8,806** CITATIONS
SEE PROFILE

Tunable Low-Field Magnetoresistance in $(La_{0.7}Sr_{0.3}MnO_3)_{0.5}$:$(ZnO)_{0.5}$ Self-Assembled Vertically Aligned Nanocomposite Thin Films

*Aiping Chen, Zhenxing Bi, Chen-Fong Tsai, JoonHwan Lee, Qing Su, Xinghang Zhang, Quanxi Jia, Judith L. MacManus-Driscoll, and Haiyan Wang**

Tunable and enhanced low-field magnetoresistance (LFMR) is observed in epitaxial $(La_{0.7}Sr_{0.3}MnO_3)_{0.5}$:$(ZnO)_{0.5}$ (LSMO:ZnO) self-assembled vertically aligned nanocomposite (VAN) thin films, which have been grown on $SrTiO_3$ (001) substrates by pulsed laser deposition (PLD). The enhanced LFMR properties of the VAN films reach values as high as 17.5% at 40 K and 30% at 154 K. They can be attributed to the spin-polarized tunneling across the artificial vertical grain boundaries (GBs) introduced by the secondary ZnO nanocolumns and the enhancement of spin fluctuation depression at the spin-disordered phase boundary regions. More interestingly, the vertical residual strain and the LFMR peak position of the VAN films can be systematically tuned by changing the deposition frequency. The tunability of the physical properties is associated with the vertical phase boundaries that change as a function of the deposition frequency. The results suggest that the tunable artificial vertical GB and spin-disordered phase boundary in the unique VAN system with vertical ferromagnetic-insulating-ferromagnetic (FM-I-FM) structure provides a viable route to manipulate the low-field magnetotransport properties in VAN films with favorable epitaxial quality.

1. Introduction

In the past decades perovskite manganites with a Curie temperature (T_C) above room temperature, such as $La_{0.7}Sr_{0.3}MnO_3$ (LSMO), exhibiting fascinating physical phenomena, including colossal magnetoresistance (CMR), magnetic anisotropy and spin-glass like behavior, have attracted much attention not only for the study of the underlying physics but also for the exploration of their potential applications.[1–3] However, the practical utilization of the CMR effect has been limited by the required high magnetic fields (several Tesla).[1,2] In the past few years the extrinsic low-field magnetoresistance (LFMR) effect, induced by spin-polarized tunneling at the grain boundaries (GBs) of polycrystalline bulk and thin-film manganites, has stimulated considerable interest as it constitutes a relatively large magnetoresistance effect in the low magnetic field (H ≤1 T) regime.[4] Grain boundaries, which decouple the neighboring ferromagnetic (FM) grains and serve as energy barriers for tunneling, are the key point for the enhanced LFMR effect.[5,6] Thus, many groups have attempted to improve the LFMR effect in manganite-based composites by incorporating a secondary phase, which not only creates additional artificial GBs but further increases the height of the tunneling barriers because of local structural disorder, chemical disorder, and spin disorder at the phase boundaries.[7–13] Various secondary phases including insulators, semiconductor oxides, and metals have been reported earlier but mostly in the form of randomly distributed granular bulk micro/nano-composites.[7–13]

Recently, the magnetoresistance effect has been reported in several manganite composite thin films, which could be more favorable for device applications. For example, Köster et al. obtained a pronounced LFMR of 25% (0.5 T) at 4.2 K in $La_{0.7}Sr_{0.3}MnO_3$ columnar films with MgO doping.[14] Moshnyaga et al. emphasized the importance of controlling the vertical interfaces in epitaxial $(La_{0.7}Ca_{0.3}MnO_3)_{1-x}$: $(MgO)_x$ nanocomposite films.[15] Kang et al. reported a LFMR of 12% at 77 K and 1 T in $(La_{0.7}Sr_{0.3}MnO_3)_{0.5}$:$(ZnO)_{0.5}$ nanocomposite films on sapphire substrates.[16]

As LFMR is largely controlled by interfacial and GB effects, significantly enhanced LFMR may be achieved in two-phase vertically aligned nanocomposite (VAN) films with well-ordered vertical phase boundaries. The formation of VAN

A. Chen, Z. Bi, C.-F. Tsai, J. H. Lee, Q. Su, Prof. H. Wang
Department of Electrical and Computer Engineering
Texas A&M University
College Station, TX 77843, USA
E-mail: wangh@ece.tamu.edu
Prof. X. Zhang
Department of Mechanical Engineering
Texas A&M University
College Station, TX 77843, USA
Dr. Q. X. Jia
Center for Integrated Nanotechnologies (CINT)
Los Alamos National Laboratory
Los Alamos, NM, 87545, USA
Dr. J. L. MacManus-Driscoll
Department of Materials Science and Metallurgy
University of Cambridge
Pembroke Street, Cambridge, CB2 3QZ, UK

DOI: 10.1002/adfm.201002746

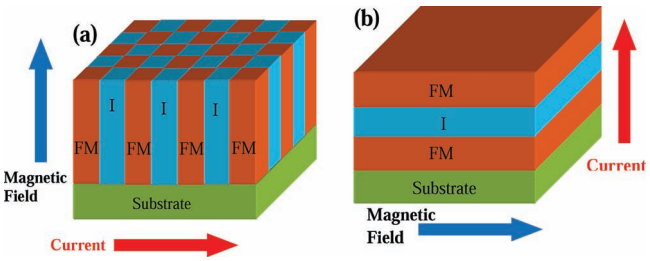

Figure 1. a) Schematic diagram of a self-assembled vertically aligned nanocomposite film with vertical ferromagnetic-insulating-ferromagnetic (FM-I-FM) tunneling structure where "FM" and "I" stand for ferromagnetic and insulating nanocolumns, respectively. b) Illustration of a conventional thin-film planar tunneling junction with FM-I-FM structure. The blue arrows indicate the applied magnetic field direction and the red arrows represent the applied current direction.

structures is related to the minimization of the relative interfacial and elastic strain energies between the two phases and between each phase and the substrate.[17,18] The VAN architecture has been reported in $BiFeO_3$:Sm_2O_3, $BiFeO_3$:$NiFe_2O_4$, and $BaTiO_3$:$CoFe_2O_4$ systems with vertical strain tuning, vertical interfacial coupling, and, thus, unique functionalities.[17–22] In addition, a thin-film solid oxide fuel cell with a VAN interlayer of $La_{0.5}Sr_{0.5}CoO_3$:$Ce_{0.9}Gd_{0.1}O_{1.95}$ has demonstrated a significantly enhanced power performance.[23] By selecting two appropriate phases for the VAN structure, it is possible to grow a vertically aligned ferromagnetic-insulating-ferromagnetic (FM-I-FM) tunneling structure in an epitaxial thin-film form. A schematic sketch of the VAN with the proposed FM-I-FM tunneling structure is given in **Figure 1**a. The vertical FM-I-FM structure in 3D is comparable to conventional thin-film tunneling junctions with a planar FM-I-FM structure, as shown in Figure 1b. In addition, using this VAN structure, it is possible to control the vertical phase boundaries in a systematic way to achieve desired and tunable LFMR at different temperatures.

In this paper, we report the growth of $(La_{0.7}Sr_{0.3}MnO_3)_{0.5}$:$(ZnO)_{0.5}$ (LSMO:ZnO) self-assembled VAN films on $SrTiO_3$ (STO) (001) substrates whereby the LSMO and ZnO nanocolumns are grown alternately and vertically aligned on the substrate. The magnetotransport properties of these LSMO:ZnO VAN thin films were measured. An enhanced and tunable LFMR effect is demonstrated in this unique vertical FM-I-FM structure. More interestingly, the LFMR can be systematically tuned by simply varying the deposition frequency. We correlate the tunable and enhanced LFMR properties to the well-controlled vertical GBs and phase boundaries using a systematic microstructure and magnetotransport property analysis.

2. Results and Discussion

Figure 2a shows the X-ray diffraction (XRD) pattern for one of the VAN films grown at 10 Hz. It is obvious that the LSMO phase in VAN films has grown in a highly textured manner along the (00*l*) direction and the ZnO phase has grown along the $(11\bar{2}0)$ direction. There are no other peaks identified as LSMO and ZnO in the complete XRD θ-2θ scan. XRD patterns of local regimes near the STO (001) peak and near the ZnO $(11\bar{2}0)$ peak of the VAN films, as illustrated in Figure 2b, show a peak shift as a function of deposition frequency and compared to that of the epitaxial LSMO film. The out-of-plane lattice parameter of the pure LSMO film, $d_{(001)LSMO}$, was determined to be 3.855 Å, which is smaller than the bulk value of 3.870 Å. This can be explained by the fact that the film is in tension in-plane because of the larger lattice of the STO substrate ($d_{(100)STO}$ = 3.905 Å) and, thus, the pure LSMO film is in compression out-of-plane. It should be noted that the $d_{(001)LSMO}$ values of the VAN films are larger than those in bulk, indicating that the vertical strain state of LSMO in the VAN films switches from compression to tension by the incorporation of the ZnO phase. It is interesting to note that the LSMO (001) peak in the VAN films gradually shifts towards larger angles and the ZnO $(11\bar{2}0)$ peak shifts towards lower angles with increasing deposition frequency. The vertical strain control in a VAN film, which is different from conventional substrate strain control, has been demonstrated in previous reports.[18–20] This interesting vertical strain in LSMO:ZnO system stems from the out-of-plane lattice matching of 5 LSMO (001) planes with 6 ZnO $(11\bar{2}0)$ planes. Figure 2c illustrates the systematic variation of out-of-plane lattice parameters for $d_{(001)LSMO}\times5$ and $d_{(11\bar{2}0)ZnO}\times6$ as a function of deposition frequency. It is clear that $d_{(001)LSMO}\times5$ is slightly smaller than $d_{(11\bar{2}0)ZnO}\times6$ which explains why LSMO is in tension out-of-plane. As the deposition frequency increases, $d_{(001)LSMO}\times5$ reduces gradually whereas $d_{(11\bar{2}0)ZnO}\times6$ increases, which leaves large differences in the vertical lattice parameters,

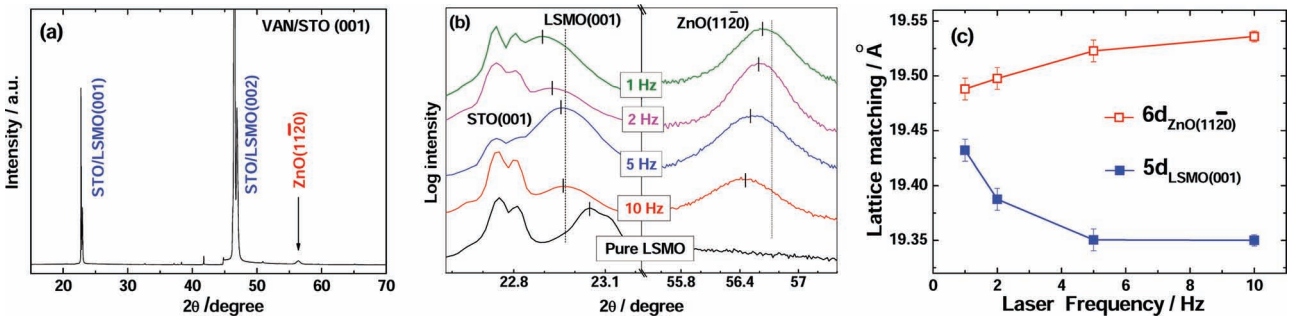

Figure 2. a) XRD of 10 Hz VAN film grown on STO (001) substrate. b) Local XRD θ-2θ scans of VAN films deposited at different deposition frequencies. The dashed lines represent the corresponding bulk peak position. c) Out-of-plane lattice parameters of 5 $d_{(001)LSMO}$ and 6 $d_{(11\bar{2}0)ZnO}$ versus deposition frequency.

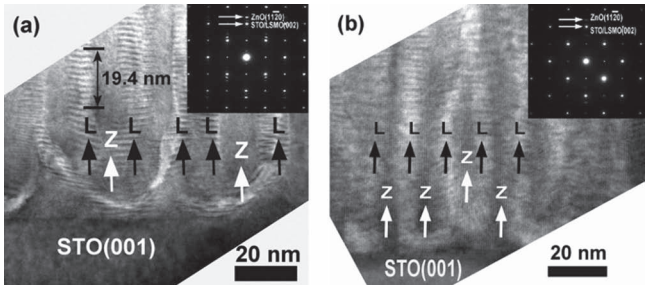

Figure 3. a) Cross-sectional TEM image of the LSMO:ZnO VAN film deposited at 1 Hz. The marked distance is 10 domain periods (19.4 nm) along the vertical interface. "Z" stands for ZnO phase and "L" represents the LSMO phase. b) TEM image of the 10 Hz VAN film on an STO substrate. The insets are the corresponding SAED patterns from the films.

in other words, a higher residual strain is induced in the vertical direction in the 10 Hz sample. The larger vertical strain observed in VAN films deposited at higher frequencies is directly related to the difference in the microstructure of the films, as will be discussed further.

To investigate the difference in microstructure of self-assembled LSMO:ZnO VAN films, we performed a detailed cross-sectional transmission electron microscopy (TEM) study on all the samples deposited at different frequencies. **Figure 3**a and b shows the cross-sectional TEM images of the films deposited at 1 Hz and 10 Hz, respectively, with the corresponding selected-area electron diffraction (SAED) pattern as inset. For both samples, the LSMO and ZnO domains have grown alternately and vertically aligned with a column size varying from around 10 nm for the 1 Hz sample to about 7 nm for the 10 Hz sample, indicating that the VAN films are self-assembled. The orientation relations between the VAN films and the substrates are determined to be $(001)_{LSMO}//(11\bar{2}0)_{ZnO}//(001)_{STO}$, $[100]_{LSMO}//[100]_{STO}$, and $[0001]_{ZnO}//[110]_{STO}$. The 45° rotation of ZnO on STO allowed the in-plane lattice matching of $d_{(1\bar{1}00)\,ZnO}\times\sqrt{2}/2$ (3.99 Å) and $d_{(100)STO}$ (3.905 Å). It is very interesting to note that the LSMO in the VAN film deposited at 1 Hz along the vertical direction exhibits a well-defined domain matching period of around 19.4 Å (as marked in Figure 3a). The ordering along the vertical domains is further evidenced by the corresponding superlattice diffraction pattern (see the inset of Figure 3a). This corresponds to a vertical lattice matching between 5 of $d_{(001)LSMO}$ and 6 of $d_{(11\bar{2}0)ZnO}$ observed in the XRD results. It can be seen in Figure 3b that the domain ordering and superlattice diffraction pattern are less obvious in the 10 Hz sample and the interfaces are less pronounced, indicating the presence of a large amount of structural and chemical disorders at the GBs and phase boundaries. The decrease in domain size (i.e., increase in the amount of vertical boundaries) and increased structural disorder at the GBs both contribute to the increase of the vertical residual strain observed in the samples deposited at higher deposition frequencies.

To be able to directly correlate the structure-property variation as a function of the deposition frequency, transport measurements were conducted for all the samples. The temperature dependence of the normalized zero-field resistivity $\rho/\rho(20\ K)$ of the LSMO:ZnO VAN films and pure epitaxial LSMO films are compared in **Figure 4**a. A well-defined metal-insulator-transition (MIT) can be observed in all the films with a systematic shift of the MIT temperature, T_{MI}, from 180 K to 290 K as the deposition frequency decreases. The temperature dependence of the magnetization was conducted for all samples and one such example (10 Hz VAN film) is shown in the inset of Figure 4b. The field-cooling (FC) curve increases continuously with decreasing temperature, whereas the zero-field-cooling (ZFC) curve exhibits a peak at the freezing temperature (T_f = 200 K) and below T_f the magnetization decreases continuously as the temperature decreases. The divergence between the FC and ZFC of VAN films usually indicates a spin-glass like behavior.[24] The frequency dependency of T_C (defined as the temperature where dM/dT reaches the minimum value) and T_{MI} are shown in Figure 4b. The same parameters for a pure LSMO film are also shown for comparison (**Table 1**) (T_C and T_{MI} of the pure epitaxial LSMO film are almost independent of the deposition frequency). The T_C of the epitaxial LSMO film is around 350 K, which is comparable to that in other reports.[18] All VAN films show a slightly reduced T_C compared to the epitaxial LSMO film, which can be explained by the suppressed double exchange (DE) interaction between the neighboring LSMO grains. The epitaxial LSMO film exhibits a characteristic T_{MI} around 344 K, which coincides with T_C (350 K), as expected, because based on DE theory the metallicity occurs at the onset of ferromagnetism in single crystals. It is interesting to note that both the T_C and T_{MI} of VAN films gradually decrease with increasing deposition frequency. The downshift of T_C and T_{MI} has also been previously observed in manganite composites with increasing concentration of the secondary phase, which was explained by the effect of enhanced GBs.[25,26] In addition, the increasing difference between T_C and T_{MI} indicates a decrease in grain size as the deposition frequency increases.[27]

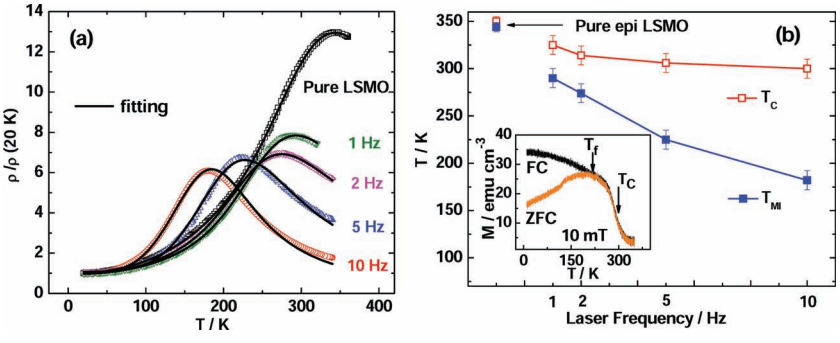

Figure 4. a) Temperature dependence of the normalized zero-field resistivity $\rho/\rho(20\ K)$ of the VAN films and of pure epitaxial LSMO films. The black solid lines are the fitted results based on the parallel connection channel model. b) Frequency dependence of T_C and T_{MI} of the VAN films. The open square (□) and closed square (■) at the upper left corner represent the parameters of pure epitaxial LSMO films. Inset: *M-T* data of 10 Hz VAN film measured under both ZFC and FC using a magnetic field of 10 mT.

Table 1. Parameters describing the properties of pure epitaxial LSMO film and $(La_{0.7}Sr_{0.3}MnO_3)_{0.5}$:$(ZnO)_{0.5}$ VAN films: T_C is the Curie temperature, T_{MI} represents the MIT temperature, T_P denotes the MR peak temperature, ΔT_{MI} is the difference of T_{MI} under a magnetic field (1 T) and zero field, G corresponds to the geometrical factor fitting from Figure 4a.

Sample	T_C [K]	T_{MI} [K]	T_P [K]	MR at T_P (0.3 T/1 T) [%]	ΔT_{MI} [K]	G
Pure LSMO	350	344	280	3.8/6.4	5	0
VAN(1 Hz)	325	290	241	5.5/9.5	8	1.42
VAN (2 Hz)	314	274	217	5.4/10.2	10.9	2.63
VAN (5 Hz)	306	225	187	8.6/18	12	5.03
VAN (10 Hz)	300	182	154	11/30	16	14.6

A parallel connection channel model has been proposed to simulate the *R-T* curves in manganite-based composite. The resistivity of the VAN system in the whole temperature regimes is given by[27–29]

$$\frac{1}{\rho} = \frac{G}{\rho_i} + \frac{1}{\rho_{LSMO}} \quad (1)$$

where ρ_i and ρ_{LSMO} denote the resistivity for the insulator phase channel and spin-polarization tunneling channel, respectively. G is the geometrical factor that rates the relative contributions from the insulator channel and spin-polarization tunneling channel. A thermally activated conduction mechanism was used to model the second phase domains and disordered phase boundary regions with $\rho_i = \exp(\Delta E_a/k_B T)$. ΔE_a is the effective activation energy for the insulator phase and disordered phase boundary regions, k_B is the Boltzmann constant, and T is the absolute temperature. In order to precisely characterize the transport properties of LSMO over the whole temperature regime, the resistivity of LSMO is modeled by a phenomenological model based on the dynamic phase segregation. The total resistivity of LSMO, the sum of resistivity in the FM domains and paramagnetic (PM) domains, is given by[30]

$$\rho_{LSMO} = (1 - f) \times \rho_{PM} + f \times \rho_{FM} \quad (2)$$

where f is the volume fraction of the FM domain in LSMO grains, and ρ_{PM} and ρ_{FM} correspond to the resistivity of the PM and FM domains in LSMO grains, respectively. The volume fraction f over the whole temperature regime is then given by[30]

$$f = \frac{1}{1 + e^{\frac{U(T/T_C - 1)}{k_B T}}} \quad (3)$$

FM domains show metallic behavior at low temperature regimes and ρ_{FM} is given by $\rho_A + \rho_B T^{2.5}$.[31] The parameter ρ_A corresponds to the residual resistivity arising from defect scatterings such as GBs and domain boundaries. The second term of ρ_{FM} represents a combination of electron-electron, electron-phonon, and electron-magnon scattering.[31] PM domains show insulating behavior and $\rho_{PM} = \exp(\Delta E_{PM}/k_B T)$, whereby ΔE_{PM} is the effective activation energy for the PM domains. Satisfactory fitting of normalized *R-T* curves (represented by solid lines in Figure 4a) by Equation 1 provides an activation energy ΔE_a of about 128 meV, ΔE_{PM} of about 99 meV, ρ_A = (0.97-1.06) and $\rho_B = (2.8–5.1) \times 10^{-6}/K^{2.5}$ (Table S1, Supporting Information). It is very interesting to find that the geometrical factor gradually increases from 1.4 to 14.6 with increasing deposition frequency from 1 Hz to 10 Hz, indicating that the effective cross-section of the insulator phase channels is greatly enhanced. It can be qualitatively explained by the variation in microstructure of the VAN films. On the one hand, the diameter of the FM grains (d_{FM}) and of the insulator grains (d_I) gradually decrease with increasing deposition frequency, which increases the density of the phase boundaries. On the other hand, the disordered region thickness ($d_{FM\text{-}I}$) tends to increase with deposition frequency, creating a "ferromagnetic-insulator" (FM-I) state consisting of spin-disordered LSMO "insulator" clusters along the vertical two-phase boundaries, as illustrated in **Figure 5**a and 5b. Thus, the geometrical factor, qualitatively related to the ratio of $d_I + 2d_{FM\text{-}I}$ and d_{FM}, tends to increase with deposition frequency. The large downshift of T_{MI} with deposition frequency is, therefore, related to the increase in effective cross-section of the insulator channel, that is, the increase of spin-disordered regions along the vertical phase boundaries. This conclusion is also consistent with the TEM observations. It is well known that the MIT is mainly governed by the GB regions between the FM grains whereas paramagnetic-superparamagnetic transitions are dominated by the FM grains. As the GBs and the domain width of the VAN films are dramatically modified by the deposition frequency (i.e., more GBs and higher disordering at GBs in higher frequency samples) whereas the coupling in FM grains is almost independent of the deposition frequency, one may expect that the reduction in T_{MI} is more pronounced than that of T_C with increasing deposition frequency.

The temperature dependence of the resistivity measured at different magnetic fields (0 T, 0.3 T, 1 T) and the corresponding magnetoresistance (MR) (defined as MR(%) = $\{[\rho_0–\rho_H]/\rho_0\} \times 100\%$, where ρ_0 and ρ_H are the resistivity under a zero field and magnetic field, respectively) for a pure epitaxial LSMO film and a 10 Hz VAN film are shown in **Figure 6**a and 6b, respectively. It is obvious that the epitaxial LSMO film exhibits negligible LFMR at low temperature and a small MR peak in the vicinity of T_C and T_{MI}. This suggests that the GB effect in the pure epitaxial LSMO film is very limited even though the GBs are mostly vertical. The 10 Hz VAN film, however, shows a much broader LFMR peak at a temperature, T_P, well below T_C and T_{MI} and the LFMR is much higher than that of the epitaxial LSMO film (Figure 6b). It is demonstrated that the LFMR values at 40 K are around 7.7% and 17.5% for 10 Hz VAN films measured at 0.3 T and 1 T, which are about 6.5 times and 12.1 times that

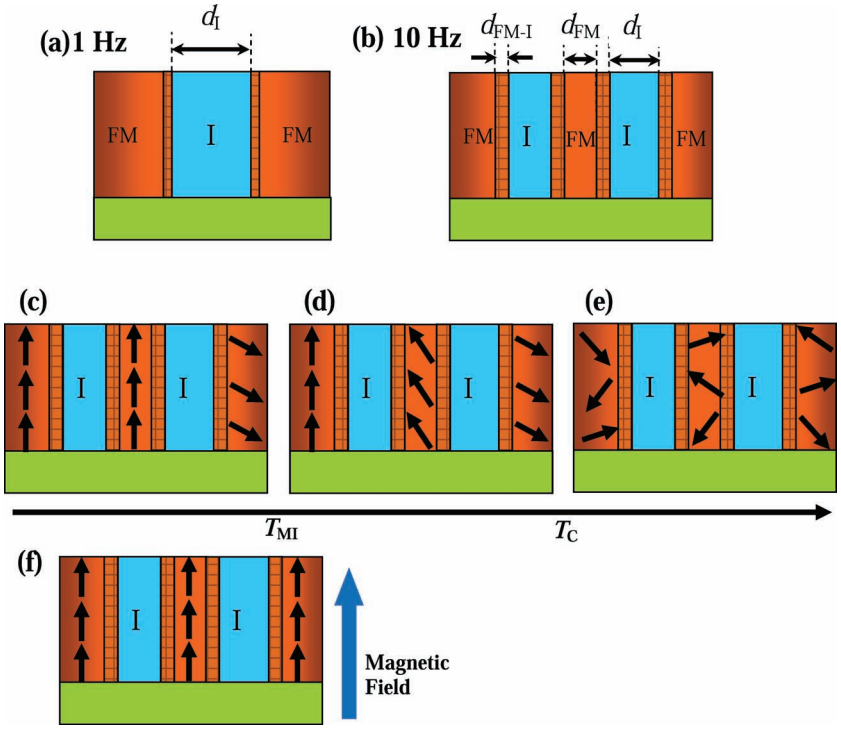

Figure 5. Schematic illustration of a highly disordered region among the vertical phase boundaries for samples deposited at: a) 1 Hz and b) 10 Hz. d_I and d_{FM} represent the thickness of the insulator and ferromagnetic phases, respectively. d_{FM-I} shows the thickness of the spin-disordered ferromagnetic-insulator region. A higher deposition frequency results in larger disordered regions and more phase boundaries. c–e) Schematic magnetic configurations of the 10 Hz VAN structure for different temperature regimes: e) The VAN system is paramagnetic at temperatures higher than T_C. d) Magnetic coupling happens in the FM intragrains for $T_{MI}<T<T_C$. c) Short-range ferromagnetic exchange interactions start in the FM intergrains at $T<T_{MI}$. f) Spins in each grain tend to align in an external magnetic field.

of the epitaxial LSMO film, respectively. More significantly, the LFMR peaks of the 10 Hz VAN film were obtained at about 154 K and the maximum LFMR values at 0.3 T and 1 T were 11% and 30%, respectively. This result is better than many other reports on LSMO:ZnO nanocomposite thin films and bulk composites.[11,12,16] The unique VAN structure is comparable to conventional thin-film planar tunneling junctions with FM-I-FM structures[32] despite the fact that the vertical FM–I–FM structure in the VAN films still needs to be optimized. Therefore, the controlled growth of VAN films with a single domain in an individual LSMO grain and a suitable composition at the percolation threshold is very desirable for further enhancing and tuning LFMR properties.

The MR plots at a magnetic field of 1 T for all VAN films deposited at different deposition frequencies are shown in **Figure 7**a. The LFMR of the pure LSMO film as a function of temperature is also shown for comparison. It is evident that the LFMR of the VAN films is larger than that of the pure LSMO film at low temperatures. More interestingly, the MR peak value of the VAN films increases and the peak position shifts toward lower temperatures with increasing deposition frequency. The peak LFMR value for VAN films deposited at 1 Hz, 2 Hz, 5 Hz, and 10 Hz measured at H = 1 T were 9.5%, 10.2%, 18%, and 30%, respectively. These values were also confirmed by magnetic-field dependent resistivity measurements (Figure S1, Supporting Information). The enhanced and tunable LFMR of the VAN systems close to the MIT can be explained by an enhanced spin-fluctuation depression because of the increase in spin-disordered phase boundary regions with increasing deposition frequency.

It can be seen that the LSMO:ZnO VAN systems, when lowering the temperature, undergo a paramagnetic-superparamagnetic transition at T_C where magnetic ordering happens in the FM intragrains. Then, the systems go through a superparamagnetic-ferromagnetic transition at T_{MI} where short-range magnetic coupling takes place in FM intergrains and a MIT takes place. The magnetic configurations of VAN structures in different temperature regimes are illustrated in Figure 5c, 5d, and 5e. Under a low magnetic field (see Figure 5f), intergrain spins tend to align because of the small coercive field for the domain-wall rotation, resulting in a shift of T_{MI} to higher temperatures and a dramatic drop of the resistivity near the T_{MI}. The resulting strong MR peak in the VAN system is similar to the intrinsic CMR mechanism.[4] Nevertheless, compared to a pure LSMO system, the shift of T_{MI} under a magnetic field, ΔT_{MI}, and the decrease in resistivity in the VAN systems are more prominent because of the suppressed DE interaction between the neighboring FM grains (see Table 1). Moreover, the increase in MR close to the MIT in VAN systems with increasing deposition frequency can mainly be attributed to the enhancement in spin-fluctuation depression related to the increase in spin-disorder at the phase boundaries.

In order to explore the LFMR effect at low temperatures, the resistivity ratio and magnetic hysteresis loop of the 10 Hz

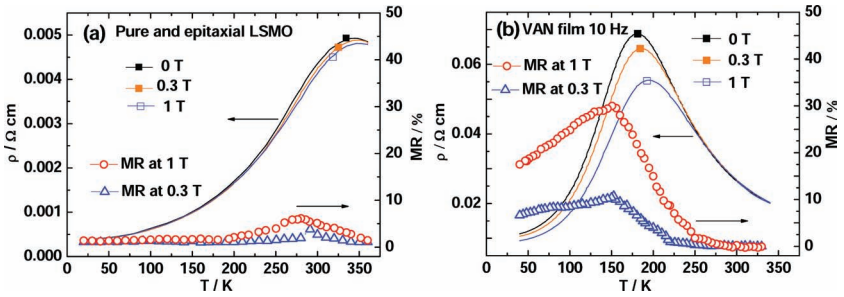

Figure 6. Temperature dependence of the resistivity for a) pure epitaxial LSMO film and b) VAN films deposited at 10 Hz measured at different magnetic fields. The open triangles (Δ) and open circles (○) represent the MR measured at 0.3 T and 1 T, respectively.

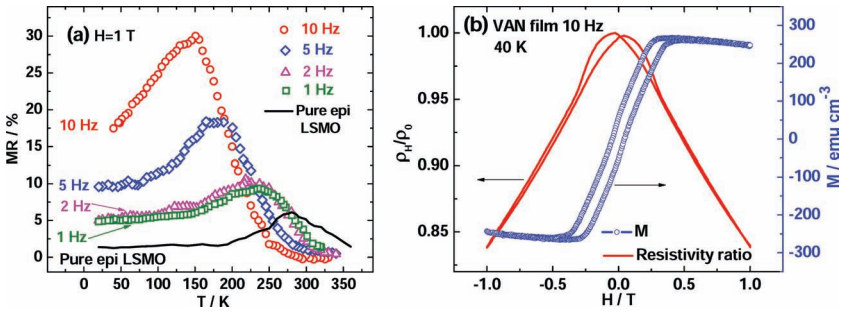

Figure 7. a) MR as a function of temperature for LSMO:ZnO VAN films deposited at different frequencies. The MR measured for an epitaxial LSMO film as a function of temperature is also shown (black solid line) for comparison. b) Resistivity ratio ρ_H/ρ_0 and magnetic hysteresis loop of 10 Hz VAN films as a function of magnetic field at a temperature of 40 K.

VAN sample were measured at 40 K as a function of magnetic field and are shown in Figure 7b. The linear slope of the out-of-plane magnetization curve indicates the reversible domain-wall motion.[33] The MR related to spin-polarized transport is given by[4]

$$MR = \frac{\rho_0 - \rho_H}{\rho_0} = \frac{J\,P}{4k_B\,T}[m^2(H,\,T) - m^2(0,\,T)] \quad (4)$$

where m represents the magnetization normalized to the saturation value; J denotes the intergrain exchange constant and P corresponds to the electron polarization. Thus, resistivity ratio ρ_H/ρ_0 is proportional to the square of normalized magnetization. It is interesting to note that a maximum in the resistivity is observed close to the coercive field and the resistivity ratio correlates well with the magnetization at low magnetic field regimes as expected for spin-polarized tunneling. Therefore, the MR of LSMO:ZnO VAN films at low temperatures can be related to the spin-polarized tunneling of the conduction electrons through vertical artificial GBs, created by the incorporation of ZnO.[16] On the one hand, the non-magnetic ZnO nanocolumns that serve as a tunneling barrier separate the neighboring FM grains and weaken the intergrain DE interaction, thus, favoring the spin-polarized intergrain tunneling. On the other hand, the nanosized LSMO and ZnO columns in the VAN films dramatically enhance the GB effect and thus enhance the LFMR effects. It also should be noted that the density and thickness of the barrier layer plays a significant role in the low-temperature MR effect. The observed increase in the LFMR effect at low temperatures in the VAN system with increasing deposition frequency can be explained by the increased contribution from the insulator channel, namely, a larger geometric factor G is found for increasing deposition frequencies.

3. Conclusions

Our study reveals that enhanced and tunable LFMR can be achieved in high-quality epitaxial LSMO:ZnO self-assembled VAN films with vertical FM-I-FM structure on STO substrates. The tunability in LFMR, vertical strain, and domain matching can be achieved by varying the deposition frequency. The tunable and enhanced LFMR properties close to the MIT in VAN systems are mainly related to the enhancement of spin-fluctuation depression due to an increase of spin-disorder at the phase boundary regions as the deposition frequency increases. The enhanced MR effect at low temperatures is attributed to spin-polarized tunneling across the vertical artificial GBs. Our results demonstrate that manipulating the strain and structure of the vertical phase interfaces in these unique VAN films with vertical FM-I-FM architecture is a viable route to tune the physical properties in nanocomposite thin films.

4. Experimental Section

The composite target for the deposition was obtained by a conventional ceramic sintering process. The LSMO powders were first synthesized from high-purity La_2O_3, $SrCO_3$, and MnO_2 reagents. The stoichiometric mixture was ground, pressed, and sintered at 1200 °C in air for 24 h. Subsequently, the calcined LSMO powders were reground with stoichiometric ZnO powders and pressed into a disk and sintered at 1300 °C for 12 h to make a $(La_{0.7}Sr_{0.3}MnO_3)_{0.5}$:$(ZnO)_{0.5}$ (1:1, molar ratio) composite target.

LSMO:ZnO VAN thin films were deposited on single-crystal STO (001) substrates by pulsed laser deposition (PLD) with a KrF excimer laser (Lambda Physik, λ = 248 nm). The laser beam was focused onto the target at an incidence angle of 45°, obtaining an energy density of approximately 4.5 J cm^{-2}. Prior to the deposition, the chamber was vacuumed to a base pressure of 1.5 × 10^{-6} Torr (1 Torr = 133.3 Pa) or better. An optimized substrate temperature of 750 °C and oxygen pressure of 200 mTorr were used during the depositions. The VAN films were deposited at 1 Hz, 2 Hz, 5 Hz, and 10 Hz, respectively. After deposition, the films were cooled down to room temperature at 20 °C min^{-1} at an oxygen pressure of 200 Torr to assure proper film oxygenation. Pure epitaxial LSMO films were also deposited on STO substrates using the same parameters for comparison.

The strain and microstructure of the films were investigated by XRD (BRUKER D8 powder X-ray diffractometer) and TEM (JEOL 2010 analytical microscope). Cross-sectional samples for TEM analysis were prepared by a standard manual grinding and thinning procedure followed by a final ion-polishing step (Gatan PIPS 691 precision ion polishing system). Au electrodes deposited by sputtering were used for the conventional four-probe resistivity measurements. The electrical properties in a temperature range of 20 K-350 K and a magnetic field up to 1 T were measured using a commercial physical properties measurement System (Quantum Design PPMS 6000). During the magnetotransport measurements, the magnetic field was applied perpendicular to the film plane and the current was performed in-plane of the film (Figure 1a). The magnetizations were measured out-of-plane by applying a magnetic field perpendicular to the film plane. In the zero-field cooling (ZFC) measurements, the samples were first cooled from 350 K to 20 K without a magnetic field, and then sequentially raised to 350 K under a magnetic field. The magnetization responses were recorded on the heating cycle. In the case of field cooling (FC), the samples were put in a field followed by cooling down to 20 K and then heating up again to 350 K, and the magnetizations were also measured during the heating cycle.

Supporting Information

Supporting Information is available from the Wiley Online Library or from the author.

Acknowledgements

The research at Texas A&M University was supported by the U.S. National Science Foundation (Ceramic Program, NSF 0709831 and NSF 1007969). The work at Los Alamos was performed, in part, at the Center for Integrated Nanotechnologies, a U.S. Department of Energy, Office of Basic Energy Sciences user facility. Los Alamos National Laboratory, an affirmative action equal opportunity employer, is operated by Los Alamos National Security, LLC, for the National Nuclear Security Administration of the U.S. Department of Energy under contract DE-AC52-06NA25396.

Received: December 29, 2010
Published online: April 26, 2011

[1] S. Jin, T. H. Tiefel, M. McCormack, R. A. Fastnacht, R. Ramesh, L. H. Chen, *Science* **1994**, *264*, 413.
[2] G. Jeffrey Snyder, R. Hiskes, S. DiCarolis, M. R. Beasley, T. H. Geballe, *Phys. Rev. B* **1996**, *53*, 14434.
[3] Y. Suzuki, H. Y. Hwang, S-W. Cheong, R. B. van Dover, *Appl. Phys. Lett.* **1997**, *71*, 140.
[4] H. Y. Hwang, S-W. Cheong, N. P. Ong, B. Batlogg, *Phys. Rev. Lett.* **1996**, *77*, 2041.
[5] R. Gross, L. Alff, B. Büchner, B. H. Freitag, C. Höfener, J. Klein, Y. Lu, W. Mader, J. B. Philipp, M. S. R. Rao, P. Reutler, S. Ritter, S. Thienhaus, S. Uhlenbruck, B. Wiedenhorst, *J. Magn. Magn. Mater.* **2000**, *211*, 150.
[6] X. L. Wang, S. X. Dou, H. K. Liu, M. Ionescu, B. Zeimetz, *Appl. Phys. Lett.* **1998**, *73*, 396.
[7] Y. M. Kang, H. J. Kim, S. I. Yoo, *Appl. Phys. Lett.* **2009**, *95*, 052510.
[8] P. K. Siwach, H. K. Singh, O. N. Srivastava, *J. Phys. Condens. Matter* **2008**, *20*, 273201.
[9] X. S. Yang, Y. Yang, W. He, C. H. Cheng, Y. Zhao, *J. Phys. D* **2008**, *41*, 115009.
[10] S. L. Young, H. Z. Chen, C. C. Lin, J. B. Shi, L. Horng, Y. T. Shih, *J. Magn. Magn. Mater.* **2006**, *303*, e325.
[11] D. Das, C. M. Srivastava, D. Bahadur, A. K. Nigam, S. K. Malik, *J. Phys. Condens. Matter* **2004**, *16*, 4089.
[12] C. S. Xiong, Y. Zeng, Y. H. Xiong, J. Zhang, Y. B. Pi, L. Zhang, J. Xiong, X. W. Cheng, F. F. Wei, L. J. Li, *Phys. B* **2008**, *403*, 3266.
[13] L. Yan, L. B. Kong, T. Yang, W. C. Goh, C. Y. Tan, C. K. Ong, Md. A. Rahman, T. Osipowicz, M. Q. Ren, *J. Appl. Phys.* **2004**, *96*, 1568.
[14] S. A. Köster, V. Moshnyaga, K. Samwer, O. I. Lebedev, G. van Tendeloo, O. Shapoval, A. Belenchuk, *Appl. Phys. Lett.* **2002**, *81*, 1648.
[15] V. Moshnyaga, B. Damaschke, O. Shapoval, A. Belenchuk, J. Faupel, O. I. Lebedev, J. Verbeeck, G. van Tendeloo, M. Mücksch, V. Tsurkan, R. Tidecks, K. Samwer, *Nat. Mater.* **2003**, *2*, 247.
[16] B. S. Kang, H. Y. Wang, J. L. MacManus-Driscoll, Y. Li, Q. X. Jia, I. Mihut, J. B. Betts, *Appl. Phys. Lett.* **2006**, *88*, 192514.
[17] J. L. MacManus-Driscoll, *Adv. Funct. Mater.* **2010**, *20*, 2035.
[18] J. L. MacManus-Driscoll, P. Zerrer, H. Y. Wang, H. Yang, J. Yoon, A. Fouchet, R. Yu, M. G. Blamire, Q. X. Jia, *Nat. Mater.* **2008**, *7*, 314.
[19] H. Yang, H. Y. Wang, J. S. Yoon, Y. Q. Wang, M. K. Jain, D. M. Feldmann, P. C. Dowden, J. L. MacManus-Driscoll, Q. X. Jia, *Adv. Mater.* **2009**, *21*, 3794.
[20] Z. X. Bi, J. H. Lee, H. Yang, Q. X. Jia, J. L. MacManus-Driscoll, H. Y. Wang, *J. Appl. Phys.* **2009**, *106*, 094309.
[21] Q. Zhan, R. Yu, S. P. Crane, H. Zheng, C. Kisielowski, R. Ramesh, *Appl. Phys. Lett.* **2006**, *89*, 172902.
[22] H. Zheng, J. Wang, S. E. Lofland, Z. Ma, L. Mohaddes-Ardabili, T. Zhao, L. Salamanca-Riba, S. R. Shinde, S. B. Ogale, F. Bai, D. Viehland, Y. Jia, D. G. Schlom, M. Wuttig, A. Roytburd, R. Ramesh, *Science* **2004**, *303*, 661.
[23] J. S. Yoon, S. M. Cho, J.-H. Kim, J. H. Lee, Z. Bi, A. Serquis, X. Zhang, A. Manthiram, H. Y. Wang, *Adv. Funct. Mater.* **2009**, *19*, 3868.
[24] C. S. Xiong, Y. H. Xiong, W. Yi, G. N. Meng, Z. C. Xia, X. G. Li, S. L. Yuan, *J. Phys. Condens. Matter* **2002**, *14*, 4309.
[25] H. Yang, Z. E. Cao, X. Shen, T. Xian, W. J. Feng, J. L. Jiang, Y. C. Feng, Z. Q. Wei, J. F. Dai, *J. Appl. Phys.* **2009**, *106*, 104317.
[26] J. Y. Gu, C. Kwon, M. C. Robson, Z. Trajanovic, K. Ghosh, R. P. Sharma, R. Shreekala, M. Rajeswari, T. Venkatesan, R. Ramesh, T. W. Noh, *Appl. Phys. Lett.* **1997**, *70*, 1763.
[27] S. L. Yuan, Z. C. Xia, L. Liu, W. Chen, L. F. Zhao, J. Tang, G. H. Zhang, L. J. Zhang, H. Cao, W. Feng, Y. Tian, L. Y. Niu, S. Liu, *Phys. Rev. B* **2003**, *68*, 184423.
[28] LI. Balcells, A. E. Carrillo, B. Martínez, J. Fontcuberta, *Appl. Phys. Lett.* **1999**, *74*, 4014.
[29] A. de Andrés, M. García-Hernández, J. L. Martínez, *Phys. Rev. B* **1999**, *60*, 7328.
[30] S. L. Yuan, Z. Y. Li, W. Y. Zhao, G. Li, Y. Jiang, X. Y. Zeng, Y. P. Yang, G. Q. Zhang, F. Tu, C. Q. Tang, S. Z. Jin, *Phys. Rev. B* **2001**, *63*, 172415.
[31] P. Schiffer, A. P. Ramirez, W. Bao, S.-W. Cheong, *Phys. Rev. Lett.* **1995**, *75*, 3336.
[32] J. S. Moodera, L. R. Kinder, T. M. Wong, R. Meservey, *Phys. Rev. Lett.* **1995**, *74*, 3273.
[33] Y. Wu, Y. Suzuki, U. Rüdiger, J. Yu, A. D. Kent, T. K. Nath, C. B. Eom, *Appl. Phys. Lett.* **1999**, *75*, 2295.